

Minimal Adversarial Examples for Deep Learning on 3D Point Clouds

Jaeyeon Kim¹ Binh-Son Hua^{2,3} Duc Thanh Nguyen⁴ Sai-Kit Yeung¹

¹Hong Kong University of Science and Technology

²VinAI Research, Vietnam

⁴Deakin University

³VinUniversity, Vietnam

Abstract

With recent developments of convolutional neural networks, deep learning for 3D point clouds has shown significant progress in various 3D scene understanding tasks, e.g., object recognition, object detection. In a safety-critical environment, it is however not well understood how such deep learning models are vulnerable to adversarial examples. In this work, we explore adversarial attacks for point cloud-based neural networks. We propose a general formulation for adversarial point cloud generation via ℓ_0 -norm optimisation. Our method generates adversarial examples by attacking the classification ability of the point cloud-based networks while considering the perceptibility of the examples and ensuring the minimum level of point manipulations. The proposed method is general and can be realised in different attack strategies. Experimental results show that our method achieves the state-of-the-art performance with higher than 89% and 90% of attack success on synthetic and real-world data respectively, while manipulating only about 4% of the total points.

1. Introduction

Deep learning has shown great potentials in solving a wide spectrum of computer vision tasks. In life-crucial applications, one concern is that deep neural networks can be vulnerable to adversarial examples, a special kind of inputs that can fool the networks to make undesirable predictions. Several adversarial attack techniques have been proposed to generate such examples. In contrast, adversarial defense methods have been developed to detect and neutralise adversarial examples. Therefore, understanding how adversarial attacks and defenses operate is of great importance to make deep learning techniques more reliable and robust.

With the growing popularity of low-cost 3D sensors and light-field cameras, the community has also started investigating the vulnerability of neural networks on 3D data, especially 3D point clouds [39, 18, 19, 42, 35]. However, existing works focus on common scenarios, such as generating adversarial point clouds by perturbing points in input

point clouds. While such approaches have a high attack success rate, the perturbations are not imperceptible and can be identified easily by outlier detection or noise removal algorithms. In addition, existing adversarial attack methods do not perform optimally since all points in a point cloud are involved in the manipulation.

In this work, we investigate 3D adversarial attacks in more extreme but practical settings. First, we explore how to generate adversarial point clouds such that the number of points perturbed from an original point cloud is minimal while maintaining the perceptibility of the point cloud. We propose a new formulation for adversarial point cloud generation that can be adapted to different attack strategies. Second, we conduct a vulnerability analysis on the relation between the perturbed points found by our method and the concept of critical points in PointNet [26]. Third, we explore adversarial attacks to point clouds obtained from both synthetic and real-world 3D scans. In summary, our contributions include:

- A new technique to generate minimal adversarial point clouds. We formulate the problem using ℓ_0 -norm optimisation that can then be approximately solved by ℓ_1 -norm optimisation;
- A new theoretical formulation that generalises two adversarial point clouds generation techniques: point perturbation and point addition;
- A vulnerability analysis on perturbed and critical points;
- A benchmark of adversarial attacks on both synthetic and real-world 3D point clouds, which shows our method achieves consistent performance over both domains.

2. Related Work

3D Deep Learning. Recent availability of 3D datasets [38, 5, 13, 2, 7, 4, 33] has led to significant advances in deep learning on 3D data. In this domain, most existing works focus on designing convolution operations that enable convolutional neural networks to learn features directly from point

clouds [26, 27, 17, 40, 14, 34, 30, 15, 46]. Several attempts have been made to create rotation invariant convolutions [28, 45, 25, 43]. Such convolutions allow scene understanding tasks, e.g., object recognition, semantic segmentation, and object detection, to be trained directly with various input point clouds. Other improvements have also been found in the literature. For instance, Liu et al. [20] proposed an RNN-based model to extract the correlations of local areas. Yan et al. [41] extended the pointwise MLP network by adopting adaptive sampling to handle outliers and noise.

In this work, we adopt PointNet [26] as a target neural network to attack. We run experiments on ModelNet40 [38] and ScanObjectNN [33]. ModelNet40 contains a collection of CAD models used for benchmarking state-of-the-art object classification techniques. ScanObjectNN is a dataset of real-world 3D point clouds designed to further benchmark the performance of object classification. We also verify our method with different deep learning models including PointNet++ [27], DGCNN [34], SpiderCNN [40], and PointASNL [41].

Adversarial Point Clouds. There exist studies on adversarial attacks and defenses for point cloud classification [39, 18, 19, 42, 47, 32, 12, 49, 16]. For instance, Xiang et al. [39] proposed an algorithm for point perturbation and addition based on the attack framework in [3] using Chamfer and Hausdorff distance. Liu et al. [18] extended the fast gradient sign method in [11] for constructing 3D adversarial examples using mesh and clipping norm. In general, the basic ideas in these works follow previous adversarial attack techniques in 2D domain, which focus on how a point cloud should be perturbed to make an adversarial example. Readers are referred to [44] for a comprehensive review on adversarial attacks and defenses on images.

It is also possible to mix newly added points with perturbed points in a point cloud to make adversarial examples [19]. Yuxin et al. [35] considered the consistency of local curvatures in a loss function to guide perturbed points lean towards object surfaces. Tsai et al. [32] incorporated the K-Nearest Neighbor loss in [39] to constrain adversarial samples to become physical objects. Zhao et al. [47] showed the vulnerability of isometry transformation by making perturbations on isometry matrix. Hadmi et al. [12] proposed the use of auto-encoders in perturbation to improve the transferability of adversarial examples across different deep neural networks. Lee et al. [16] added perturbation noise into the latent space of auto-encoders to maintain the shape of input point clouds. Zhou et al. [49] employed GAN [10] in generating adversarial point clouds with predefined target labels.

In addition to creating adversarial examples by perturbing existing points or adding new points into point clouds,

one can fool classification techniques by removing points from input data [48, 36, 42]. For instance, Zheng et al. [48] eliminated important points on saliency map of an input object. Matthew et al. [36] iteratively removed critical points from an input point cloud until a target classification technique failed to classify the point cloud.

In contrast to adversarial attacks, countermeasures for adversarial point clouds have been so far scarce. Typical defense approaches include outlier or salient point removal [18] and noise removal [42, 50]. Recently, Dong et al. [8] used relative position of each local part of a clean point cloud to global object center as adversarial indicator. Wu et al. [37] proposed a method to predict implicit functions capturing clean shapes of point clouds. Clean and complete objects of adversarial point clouds could be then restored using implicit functions.

Minimal Adversarial Attacks. In 2D domain, there is a specific family of techniques that focus on perturbing a minimum number of pixels in adversarial attacks. For instance, Papernot et al. [24] perturbed pixels on saliency maps. Carlini et al. [3] extended this method and used ℓ_0 -norm optimisation to minimise the number of pixels to perturb. Recently, Modas et al. [21] and Croce et al. [6] focused on how to perturb a sparse set of pixels while still achieving good perceptibility. Local search and evolutionary algorithms were also applied to obtain sparse perturbations in [22, 31, 29].

In this paper, we also explore adversarial attacks that only manipulate a minimal set of points. However, unlike the above works, we propose a new formulation that is general and can be adapted to various adversarial point cloud generation strategies. In addition, we also consider the perceptibility of adversarial examples in our formulation.

3. Proposed Method

We propose a general formulation for adversarial attacks to 3D point clouds using ℓ_0 -norm optimisation. We show that our formulation can be adapted to various settings and realised in different attack strategies.

Our problem of interest can be stated as follows. Let $P = \{\mathbf{p}_1, \dots, \mathbf{p}_N\}$ be an input set of N points where each point \mathbf{p}_i is represented by a vector of its coordinates $\mathbf{p}_i = [p_{i,x}, p_{i,y}, p_{i,z}]^\top \in \mathbb{R}^3$. Let F denote a point-based neural network, e.g., PointNet [26], and $F_i(P)$ denote the probability that the point set P is classified into the i -th class or the i -th element of the logits in a softmax layer. If i^* is the true class label of the point cloud P , then $i^* = \arg\max_i F_i(P)$. Let P' be an adversarial example of P . We aim to find P' such that $\arg\max_i F_i(P) \neq \arg\max_{i'} F_{i'}(P')$, i.e., P' and P are classified into different classes by the network F .

In the following, we present a general model to generate P' using ℓ_0 -norm optimisation and describe in details two different ways to realise our model: point perturbation and point addition.

3.1. Point Perturbation

3.1.1 Formulation

Given a point cloud P , we aim to find a minimal set of points that can be shifted to generate an adversarial point cloud P' to attack the network F . In this case, the adversarial point cloud P' generated by the point perturbation process will have the same number of points (with P). Intuitively, the point perturbation process must satisfy the following conditions: (i) the perceptibility of the point cloud is maintained during the perturbation, i.e., the perturbed point cloud P' should not much deform from the original point cloud P ; (ii) a minimal number of points in P are selected for perturbation; and (iii) the original point cloud P and perturbed point cloud P' are classified into different classes by the network F .

We express the selection of points in P for perturbation by a binary indication vector $\mathbf{a} = [a_1, \dots, a_N]^\top \in \{0, 1\}^N$ where a_i is 1 if \mathbf{p}_i is selected, and 0 otherwise. Suppose that $E = \{\mathbf{e}_1, \dots, \mathbf{e}_N\}$ is the set of perturbations, in which $\mathbf{e}_i = [e_{i,x}, e_{i,y}, e_{i,z}]^\top \in \mathbb{R}^3$ is the perturbation vector to be applied on \mathbf{p}_i to obtain \mathbf{p}'_i . Applying perturbation set E on the point cloud P results in an adversarial point cloud P' as

$$P' = \{\mathbf{p}'_i = \mathbf{p}_i + a_i \mathbf{e}_i \mid \mathbf{p}_i \in P\}. \quad (1)$$

The process of generation of P' can be formulated as,

$$\begin{aligned} \min_{\mathbf{a}, E} f(P, \mathbf{a}, E) &= \min_{\mathbf{a}, E} \{\lambda_1 \|\mathbf{a}\|_0 + \lambda_2 D(P, P')\} \\ \text{s.t.} \quad \arg\max_i F_i(P) &\neq \arg\max_{i'} F_{i'}(P') \end{aligned} \quad (2)$$

where $\|\mathbf{a}\|_0 = \#\{i : a_i \neq 0, i = 1, \dots, N\}$ is the ℓ_0 -norm of \mathbf{a} (i.e., the number of non-zero elements in \mathbf{a}) and $D(P, P')$ is some distance between P and P' .

The optimisation problem defined in Eq. (2) covers all the aforementioned conditions. In particular, the first term, $\|\mathbf{a}\|_0$ in the objective function $f(P, \mathbf{a}, E)$ imposes the quantity of selected points in the point selection process while the second term, $D(P, P')$ constrains the perceptibility of the adversarial point cloud P' w.r.t. the original point cloud P . As will be explained later in this section, $D(P, P')$ can be defined using different distance metrics. The constraint $\arg\max_i F_i(P) \neq \arg\max_{i'} F_{i'}(P')$ ensures the generated point cloud P' can fool the network F , i.e., F would not classify P and P' into the same class.

3.1.2 Perceptibility

There are several ways to realise the perceptibility $D(P, P')$ in Eq. (2). If we assume the correspondence between each

point $\mathbf{p}_i \in P$ and its perturbed point $\mathbf{p}'_i \in P'$ defined in Eq. (1) is maintained, then we can define $D(P, P')$ using the Euclidean distances between \mathbf{p}_i and \mathbf{p}'_i as,

$$D_{Euclidean}(P, P') = \frac{1}{N} \sum_{i=1}^N (a_i \|\mathbf{e}_i\|_2). \quad (3)$$

However, such correspondences are not always well defined, e.g., when the number of points changes in the case of point addition, making Euclidean distance not a valid choice. We further propose to use Chamfer distance and Hausdorff distance to measure perceptibility. Specifically, we can define $D(P, P')$ as

$$\begin{aligned} D_{Chamfer}(P, P') &= \max \left\{ \frac{1}{|P|} \sum_{\mathbf{p}_i \in P} \min_{\mathbf{p}'_j \in P'} \|\mathbf{p}_i - \mathbf{p}'_j\|_2, \right. \\ &\quad \left. \frac{1}{|P'|} \sum_{\mathbf{p}'_j \in P'} \min_{\mathbf{p}_i \in P} \|\mathbf{p}'_j - \mathbf{p}_i\|_2 \right\} \end{aligned} \quad (4)$$

or

$$\begin{aligned} D_{Hausdorff}(P, P') &= \max \left\{ \max_{\mathbf{p}_i \in P} \left\{ \min_{\mathbf{p}'_j \in P'} \|\mathbf{p}_i - \mathbf{p}'_j\|_2 \right\}, \right. \\ &\quad \left. \max_{\mathbf{p}'_j \in P'} \left\{ \min_{\mathbf{p}_i \in P} \|\mathbf{p}'_j - \mathbf{p}_i\|_2 \right\} \right\}. \end{aligned} \quad (5)$$

As shown in Eq. (4)-(5), both Chamfer distance and Hausdorff distance do not require the same of number of points in the point clouds P and P' . Hence, they can be adapted easily to different point generation methods, e.g., point addition as presented in Section 3.2.

3.1.3 Relaxed Formulation

To solve the constrained optimisation problem in Eq. (2), we convert it into an unconstrained optimisation problem using a Lagrange multiplier-like form as:

$$\begin{aligned} \min_{\mathbf{a}, E} f(P, \mathbf{a}, E) \\ = \min_{\mathbf{a}, E} \{\lambda_1 \|\mathbf{a}\|_0 + \lambda_2 D(P, P') + h(P')\} \end{aligned} \quad (6)$$

where, like [39], we define,

$$h(P') = \max \left\{ 0, F_{i^*}(P') - \max_{i^* \neq i'} F_{i'}(P') \right\} \quad (7)$$

where i^* is the true class label of the point set P .

Since the problem in Eq. (6) is NP-hard in general [23], we further relax it as ℓ_1 -norm optimisation [1, 9] as:

$$\begin{aligned} \min_{\hat{\mathbf{a}}, E} f(P, \hat{\mathbf{a}}, E) \\ = \min_{\hat{\mathbf{a}}, E} \{\lambda_1 \|\hat{\mathbf{a}}\|_1 + \lambda_2 D(P, P') + h(P')\} \end{aligned} \quad (8)$$

where $\hat{\mathbf{a}} = [\hat{a}_1, \dots, \hat{a}_N]^\top \in [0, 1]^N$, and $\|\hat{\mathbf{a}}\|_1 = \sum_{i=1}^N \hat{a}_i$ is the ℓ_1 -norm of $\hat{\mathbf{a}}$.

To solve Eq. (8), we apply the iterative gradient method in [11, 18]. Since the final aim is to obtain a binary vector for \mathbf{a} , we randomly initialise $\hat{\mathbf{a}}$ with near-binary values, i.e., \hat{a}_i is randomly set to either 0.0001 or 0.9999. Near-binary values are used to give \hat{a}_i chances to turn into 1 (or 0) if \mathbf{p}_i is selected (or otherwise). Finally, we achieve the final solution for \mathbf{a} as,

$$a_i = \begin{cases} 0, & \text{if } \hat{a}_i = 0 \\ 1, & \text{otherwise.} \end{cases} \quad (9)$$

Note that we aim to find solutions for both \mathbf{a} and \mathbf{e} . Given \mathbf{a} obtained from Eq. (9), we only consider perturbations \mathbf{e}_i if $a_i = 1$.

The optimisation problem defined in Eq. (8) formulates our proposed adversarial generation method. This formulation is general and can be adapted conveniently to other adversarial generation strategies, e.g., point addition.

3.2. Point Addition

In addition to point perturbation, we can generate an adversarial example P' by extending P with a minimum number of additional points. We show that our proposed formulation in Eq. (8) can also be applied in this task. Specifically, suppose that there are no more than K points added to the original point cloud P . We can construct a new point set \tilde{P} including all the points in P and K new points. These K new points can be generated by randomly choosing K points in P and adding them to \tilde{P} . We note that this way of construction of \tilde{P} does not change the perceptibility of P as $D(P, \tilde{P}) = 0$ for either the Chamfer distance or Hausdorff distance used to define $D(P, \tilde{P})$. In addition, both P and \tilde{P} are treated equally by the network F , i.e., $\forall i, F_i(P) = F_i(\tilde{P})$, as the geometric structure of the point clouds remains unchanged.

Similarly, we also construct a vector $\tilde{\mathbf{a}} = [\tilde{a}_1, \dots, \tilde{a}_{N+K}]^\top \in [0, 1]^{N+K}$ and a perturbation set $\tilde{E} = \{\tilde{\mathbf{e}}_1, \dots, \tilde{\mathbf{e}}_{N+K}\}$ by extending \mathbf{a} and E with K new elements and solve the optimisation problem in Eq. (8) with a new objective function $f(\tilde{P}, \tilde{\mathbf{a}}, \tilde{E})$. The vector $\tilde{\mathbf{a}}$ is initialised as follows, \tilde{a}_i is set to 0 for $i \in \{1, \dots, N\}$, and to a random value in $\{0.0001, 0.9999\}$ for $i \in \{N+1, \dots, N+K\}$. Furthermore, during the optimisation process, we fix $\tilde{a}_i = 0, \forall i = 1, \dots, N$, i.e., original points in P will not be changed. Finally, the adversarial point cloud P' is obtained by including points $\tilde{\mathbf{p}}_i \in \tilde{P}$ such that $\tilde{a}_i = 1$.

4. Experiments and Results

4.1. Experiment Setup

Datasets. We experimented our method on ModelNet40 [38] and ScanObjectNN [33] dataset. ModelNet40 is a benchmark dataset for classification of 3D CAD models. It consists of 9,843 models for training and 2,468 models for testing. We followed the experimental setup in [26] to sample the surfaces of 3D models in ModelNet40 uniformly and then normalised points into a unit cube. ScanObjectNN is an object dataset from real-world indoor scans. It is designed to evaluate object classification in more practical settings that involve view occlusions and object partiality. ScanObjectNN has 15,000 objects organised in five challenging variants including objects with background, translated objects, rotated objects, and scaled objects. We followed Uy et al. [33] to normalise the point clouds containing background using mean and furthest point distance.

Implementation Details. We adopted PointNet [26] as a target network on which important experiments and analyses were conducted. We trained PointNet using the settings suggested in the original paper. To handle point clouds with varying sizes, we modified the max-pooling operator and batch norm in the network accordingly. We used Adam optimiser with learning rate of 0.01. For our adversarial attack algorithm, we performed exhaustive search for the parameters in Eq. (8) and empirically set them as $\lambda_1 = 0.15$ and $\lambda_2 = 50$. Iterative gradient method in [18] with 250 iterations was employed to solve Eq. (8).

4.2. Evaluation and Comparison

We evaluated our method based on attack success rate, perceptibility of adversarial examples, and average number of manipulated points. The perceptibility of adversarial examples was measured using Chamfer and Hausdorff distance. We report the performance of our method on ModelNet40 and ScanObjectNN dataset in Table 1 and Table 2 respectively. We note that ScanObjectNN has five different variants. In this experiment, we used ‘OBJ_BG’, the most challenging variant including objects with background.

We also compared our method with existing methods. In particular, we compared our work with the method by Xiang et al. [39], which also generated adversarial examples by point perturbation and addition. Since this method aimed for targeted attack, for fair comparison, we altered it to untargeted attack. We re-implemented the method by Liu et al. [19] which perturbed points in two manners: adversarial sink (i.e., pulling points towards a sink point) and adversarial stick (i.e., resampling points on added sticks). In addition, we evaluated the method by Wicker and Kwiatkowska [36], and by Zheng et al. [48]. Since both [36] and [48] created adversarial examples by removing points,

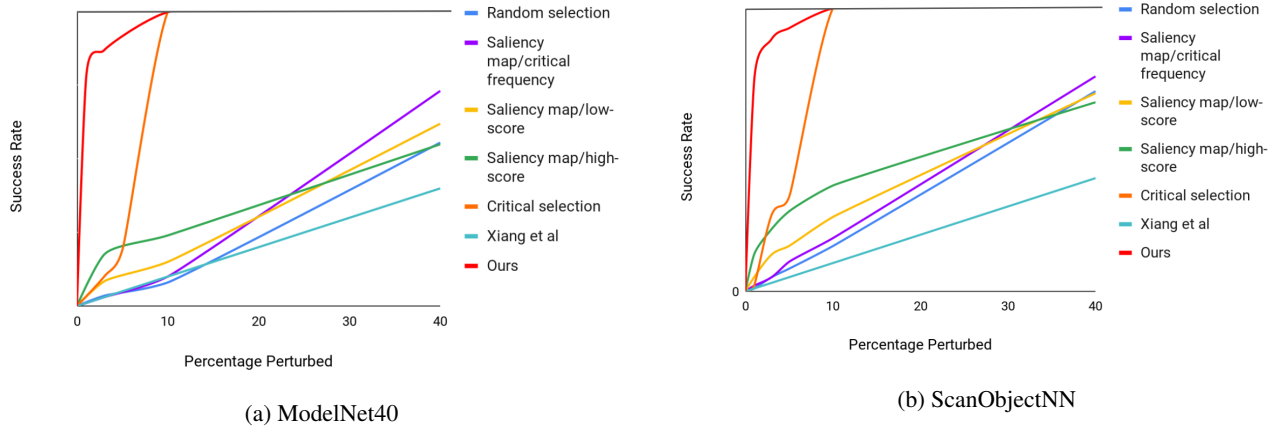


Figure 1: Performance trend of our adversarial attack and existing methods.

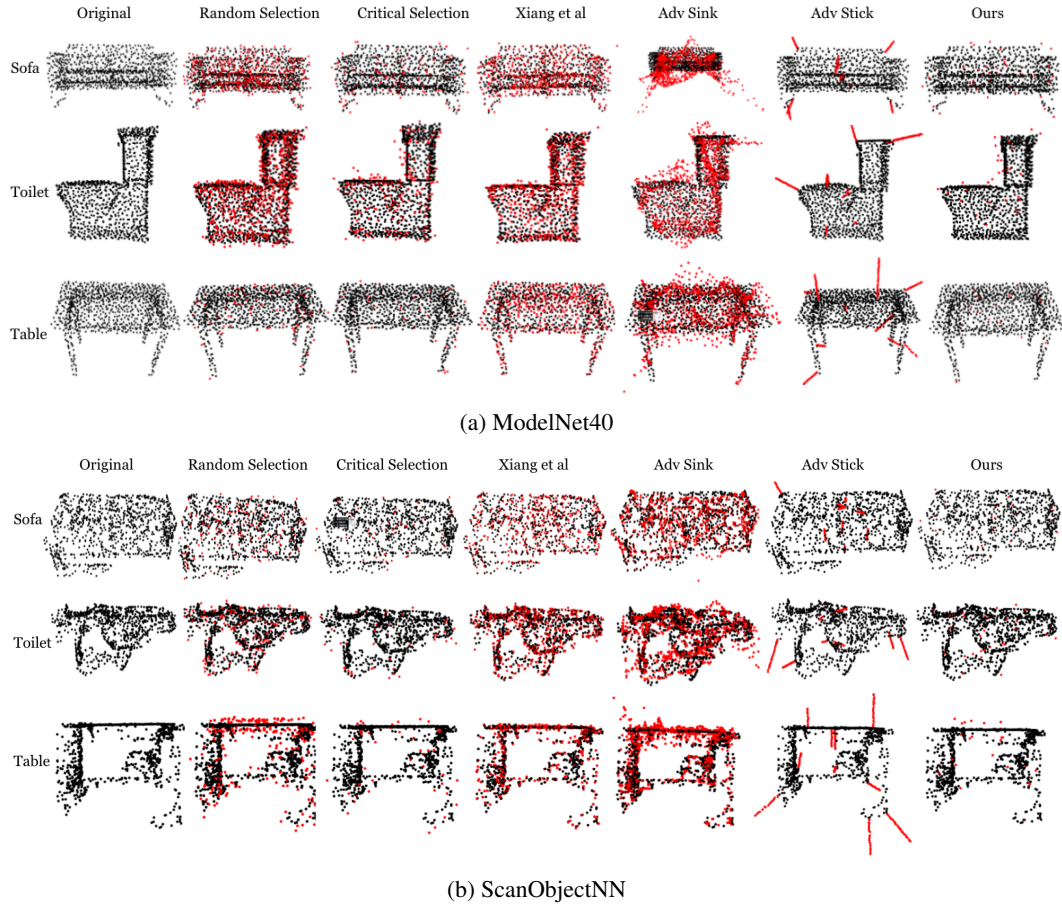


Figure 2: Adversarial examples generated by our method and existing methods. Red points represent perturbed points. On ScanObjectNN, our method is able to create examples that are indistinguishable from realistic noise.

we applied their point selection strategies but then replaced the point removal by point perturbation and point addition.

In detail, the authors in [36] selected points either randomly or from a critical point set determined by PointNet [26].

In [48], selected points were sampled from saliency maps of input point clouds in three different ways: (i) critical frequency (i.e., points frequently chosen by the max-pooling operator in PointNet [26]), (ii) low-score (i.e., points having small loss gradient for a target network), and (iii) high-score (i.e., point having large loss gradient). We will further discuss the “critical points” in Section 4.3.

As shown in Table 1 & 2, compared with other methods, our method achieves the highest success rate yet lowest number of processing points for both point perturbation and point addition, and on both ModelNet40 and ScanObjectNN. Specifically, our method uses only 4% of the total input points (1,024) to reach $> 89\%$ and $> 90\%$ of success rate on ModelNet40 and ScanObjectNN respectively. We notice that our method performs consistently (in terms of both the attack rate and the number of points) on both synthetic and real-world datasets. The adversarial sink and adversarial stick in [19] respectively take the second place w.r.t. the success rate in point perturbation on ModelNet40 and ScanObjectNN. However, both of them require great numbers of points, especially the adversarial sink. The method in [39] is ranked third for its success rate but also incurs heavy point manipulations. In addition, we observe this method often generated obvious outliers, which could be detected easily by outlier removal methods. The saliency map-based attack method [48] and the one in [36] with random point selection require roughly $10\times$ larger point sets than our method while achieving much lower success rates. The method in [36] with critical point selection shows relatively small number of points (though still more than our method), but the success rate is well below par. To further explore the performance trend, we plot the success rate over different numbers of points selected for point perturbation in Figure 1. As shown in the graphs, our method significantly outperforms existing ones with a small set of points.

Experimental results also show that our method generates highly imperceptible adversarial examples, evident by their Chamfer and Hausdorff distances to input point clouds (see Table 1 & 2). We empirically observe that using Hausdorff distance results in less outlier points than Chamfer distance. Figure 2 visualises adversarial point clouds generated by our method and other works. As shown, our method less likely produces outliers. This is due to the use of object perceptibility and minimal point set in our formula. We observe that, adversarial examples created from real-world data (see Figure 2(b)) are neither noticeable in perception nor distinguishable from common noise.

4.3. Vulnerability Analysis

Qi et al. [26] proposed a notion called “critical points” that characterise the shape of a point cloud. These points can be identified from the max pooling layer in the architecture of PointNet [26]. It is also indicated in [26] that, the criti-

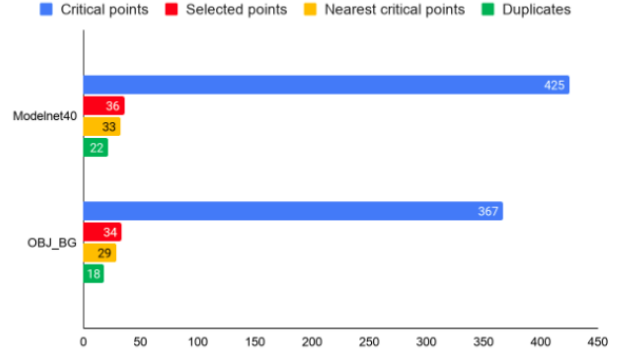


Figure 3: Our selected points vs critical points.

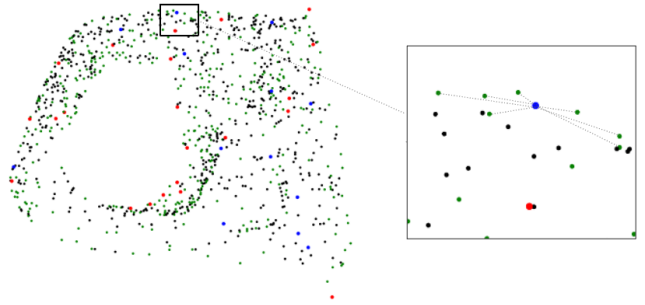


Figure 4: An adversarial example of a sink object. Original points and critical points are presented in black and green respectively. Our selected points are marked in red (if they are identical to critical points) and in blue (if they are found within the 5 nearest points of a critical point).

cal points of a point cloud play role as an indicator for the object class of the point cloud. Therefore, modification of critical points may lead to wrong classification results.

We found that our adversarial generation algorithm could somehow reach those critical points. To confirm this, we measured the coincidence of our selected points and PointNet’s critical points. Specifically, we counted the duplicates in the two point sets, and the number of our selected points found within the 5 nearest points of a critical point. Recall that our algorithm randomly initialises the selected points (i.e., the vector $\hat{\mathbf{a}}$ in Eq. (8)). Figure 3 provides the numerical data of this experiment. It is shown that about 50% of the selected points are identical to the critical points and 80% of the selected points are close to the critical points. Figure 4 visualises our selected points and critical points. As shown, our selected points are close to critical points yet occupy a small portion, proving the capability of our method of finding compact yet vulnerable point sets.

We also experimented our method with two additional initialisation schemes for the selected points: critical points-based initialisation and all point-based initialisation (i.e., taking all points in a point cloud to initialise the vector

	Success Rate	Chamfer Distance	Hausdorff Distance	# Points
Xiang et al. [39]	85.9	1.77×10^{-4}	2.38×10^{-2}	967
Adversarial sink [19]	88.3	7.65×10^{-3}	1.92×10^{-1}	1024
Adversarial stick [19]	83.7	4.93×10^{-3}	1.49×10^{-1}	210
Random selection [36]	55.56	7.47×10^{-4}	2.49×10^{-3}	413
Critical selection [36]	18.99	1.15×10^{-4}	9.39×10^{-3}	50
Saliency map/critical frequency [48]	63.15	5.72×10^{-4}	2.50×10^{-3}	303
Saliency map/low-score [48]	55.97	6.47×10^{-4}	2.50×10^{-3}	358
Saliency map/high-score [48]	58.39	7.52×10^{-4}	2.48×10^{-3}	424
Ours	89.38	1.55×10^{-4}	1.88×10^{-2}	36

(a) Point Perturbation

	Success Rate	Chamfer Distance	Hausdorff Distance	# Points
Xiang et al. [39]	73.59	7.98×10^{-3}	5.46×10^{-2}	200
Random selection [36]	43.90	2.16×10^{-4}	2.49×10^{-3}	121
Critical selection [36]	47.64	2.05×10^{-4}	2.50×10^{-3}	118
Saliency map/critical frequency [48]	45.13	2.13×10^{-4}	2.49×10^{-3}	118
Saliency map/low-score [48]	60.96	1.64×10^{-4}	2.50×10^{-3}	89
Saliency map/high-score [48]	41.06	2.27×10^{-4}	2.49×10^{-3}	128
Ours	89.01	1.53×10^{-4}	1.98×10^{-2}	38

(b) Point Addition

Table 1: Attack performance to PointNet on ModelNet40.

	Success Rate	Chamfer Distance	Hausdorff Distance	# Points
Xiang et al. [39]	81.32	1.13×10^{-4}	1.74×10^{-2}	959
Adversarial sink [19]	78.7	1.37×10^{-3}	9.81×10^{-2}	1023
Adversarial stick [19]	87.5	5.18×10^{-3}	1.67×10^{-1}	210
Random selection [36]	63.72	6.10×10^{-4}	2.50×10^{-3}	340
Critical selection [36]	47.99	1.99×10^{-4}	2.69×10^{-2}	70
Saliency map/critical frequency [48]	66.9	4.69×10^{-4}	2.50×10^{-3}	265
Saliency map/low-srop [48]	63.81	5.49×10^{-4}	2.50×10^{-3}	306
Saliency map/high-srop [48]	66.82	6.16×10^{-4}	2.47×10^{-3}	350
Ours	91.72	1.12×10^{-4}	1.15×10^{-2}	34

(a) Point Perturbation

	Success Rate	Chamfer Distance	Hausdorff Distance	# Points
Xiang et al [39]	69.26	6.07×10^{-3}	4.71×10^{-2}	200
Random selection [36]	60.05	1.77×10^{-4}	2.50×10^{-3}	97
Critical selection [36]	33.33	1.31×10^{-4}	1.84×10^{-2}	50
Saliency map/critical frequency [48]	59.63	1.79×10^{-4}	2.49×10^{-3}	97
Saliency map/low-score [48]	60.96	1.64×10^{-4}	2.50×10^{-3}	90
Saliency map/high-score [48]	57.87	1.87×10^{-4}	2.50×10^{-3}	103
Ours	90.44	1.08×10^{-4}	1.10×10^{-2}	38

(b) Point Addition

Table 2: Attack performance to PointNet on ScanObjectNN.

â). Table 3 reports the performance of various initialisation schemes. As shown in the results, the critical points-based

initialisation results in the least number of points but incurs the lowest success rate. Moreover, this scheme deterio-

	Success Rate	Chamfer Distance	Hausdorff Distance	# Points
Critical points	88.04	9.53×10^{-4}	8.28×10^{-3}	29
Using all points	91.12	1.15×10^{-4}	8.71×10^{-3}	60
Ours (random points)	90.16	1.09×10^{-4}	9.88×10^{-3}	37

Table 3: Attack performance with different initialisation strategies on ScanObjectNN.

	Success Rate	Chamfer Distance	Hausdorff Distance	# Points
Pointnet [26]	89.38	1.55×10^{-4}	1.88×10^{-2}	36
Pointnet++ [27]	88.76	5.10×10^{-4}	3.55×10^{-2}	59
DGCNN [34]	62.16	7.78×10^{-4}	3.54×10^{-2}	107
SpiderCNN [40]	89.92	4.71×10^{-4}	4.16×10^{-2}	57
PointASNL [41]	72.16	2.21×10^{-4}	2.03×10^{-2}	45

(a) Modelnet40

	Success Rate	Chamfer Distance	Hausdorff Distance	# Points
Pointnet [26]	91.72	1.12×10^{-4}	1.15×10^{-2}	34
Pointnet++ [27]	94.05	2.81×10^{-4}	2.06×10^{-2}	50
DGCNN [34]	66.46	6.80×10^{-4}	2.94×10^{-2}	103
SpiderCNN [40]	86.27	3.23×10^{-4}	2.18×10^{-2}	57
PointASNL [41]	55.88	2.07×10^{-4}	1.30×10^{-2}	47

(b) ScanObjectNN

Table 4: Attack performance to various network architectures on Modelnet40 and ScanObjectNN.

rates the perceptibility of adversarial examples (as shown in the Chamfer distances). Utilising all points for initialisation shows the opposite, i.e., more points are selected but high success rate is achieved. Our initialisation scheme compromises all the criteria, i.e., adversarial examples are created with low number of points, high attack rate, and acceptable perceptibility. In addition, random initialisation can be applied in other networks which do not support critical points.

4.4. Attack Performance to other Architectures

We also applied our adversarial example generation algorithm to attack existing point cloud architectures other than PointNet. Those architectures include PointNet++ [27], DGCNN [34], SpiderCNN [40], and PointASNL [41].

We report the attack performance of our method to these network architectures in Table 4. Amongst all the models, DGCNN [34] is shown to be the most robust one, which requires the greatest number of points to be fooled while maintaining low attack success rate. PointNet [26], on the other hand, appears to be the fragilest model, which can be fooled easily with less points to achieve high success rate. The remaining models can be attacked by slightly different numbers of points. Table 4 also shows that the attack performance of our method to a network architecture is consistent across both synthetic and real-world datasets.

5. Conclusion

In this paper, we propose a general formulation for minimal adversarial 3D point clouds generation. Our formulation can be realised into two adversarial attack strategies including point perturbation and point addition. We experimented our method on benchmark datasets, and showed that existing point cloud neural networks, e.g., PointNet, are vulnerable to attacks that perturb only 4% of the points in a point cloud to reach more than 89% and 90% of success rate on synthetic and real-world data respectively. These results pose a significant challenge in developing countermeasures to defend against such attacks.

With increasingly more 3D data used in consumer devices, we envision that adversarial attacks and defenses for point clouds will become diverse, making this topic worthy for future research. In this paper, we investigated how to perturb the 3D coordinates of a point cloud. For real-world data acquired from depth sensors, colour information is useful and could serve as an additional channel for adversarial attacks. It would be useful to study how such information influences the vulnerability of 3D deep learning. Besides, it is important to study how to create adversarial point clouds in physical world. The results of our work show that such a task could be practical as only a few percentages of an input point cloud need to be modified.

References

- [1] Edoardo Amaldi and Viggo Kann. On the approximability of minimizing nonzero variables or unsatisfied relations in linear systems. *Theoretical Computer Science*, 209(1–2):237–260, 1998.
- [2] Iro Armeni, Ozan Sener, Amir R Zamir, Helen Jiang, Ioannis Brilakis, Martin Fischer, and Silvio Savarese. 3d semantic parsing of large-scale indoor spaces. In *Computer Vision and Pattern Recognition (CVPR)*, 2016.
- [3] Nicholas Carlini and David Wagner. Towards evaluating the robustness of neural networks. In *IEEE Symposium on Security and Privacy (SP)*, 2017.
- [4] Angel Chang, Angela Dai, Thomas Funkhouser, Maciej Halber, Matthias Niessner, Manolis Savva, Shuran Song, Andy Zeng, and Yinda Zhang. Matterport3d: Learning from rgb-d data in indoor environments. *International Conference on 3D Vision (3DV)*, 2017.
- [5] Angel Chang, Thomas Funkhouser, Leonidas Guibas, Pat Hanrahan, Qi-Xing Huang, Zimo Li, Silvio Savarese, Manolis Savva, Shuran Song, Hao Su, Jianxiong Xiao, Li Yi, and Fisher Yu. Shapenet: An information-rich 3d model repository. In *arXiv:1512.03012*, 2015.
- [6] Francesco Croce and Matthias Hein. Sparse and imperceivable adversarial attacks. In *International Conference on Computer Vision (ICCV)*, 2019.
- [7] Angela Dai, Angel X Chang, Manolis Savva, Maciej Halber, Thomas Funkhouser, and Matthias Niessner. Scannet: Richly-annotated 3d reconstructions of indoor scenes. In *Computer Vision and Pattern Recognition (CVPR)*, 2017.
- [8] Xiaoyi Dong, Dongdong Chen, Hang Zhou, Gang Hua, Weiming Zhang, and Nenghai Yu. Self-robust 3d point recognition via gather-vector guidance. In *Computer Vision and Pattern Recognition (CVPR)*, 2020.
- [9] David L. Donoho and Michael Elad. Optimally sparse representation in general (nonorthogonal) dictionaries via L1 minimization. *Proceedings of the National Academy of Sciences*, 100(5):2197–2202, 2003.
- [10] Ian Goodfellow, Jean Pouget-Abadie, Mehdi Mirza, Bing Xu, David Warde-Farley, Sherjil Ozair, Aaron Courville, and Yoshua Bengio. Generative adversarial nets. In *Advances in Neural Information Processing Systems (NIPS)*, 2014.
- [11] Ian Goodfellow, Jonathon Shlens, and Christian Szegedy. Explaining and harnessing adversarial examples. In *International Conference on Learning Representations (ICLR)*, 2015.
- [12] Abdullah Hamdi, Sara Rojas, Ali Thabet, and Bernard Ghanem. Advpc: Transferable adversarial perturbations on 3d point clouds. In *European Conference on Computer Vision (ECCV)*, 2020.
- [13] Binh-Son Hua, Quang-Hieu Pham, Duc Thanh Nguyen, Minh-Khoi Tran, Lap-Fai Yu, and Sai-Kit Yeung. Scenenn: A scene meshes dataset with annotations. In *International Conference on 3D Vision (3DV)*, 2016.
- [14] Binh-Son Hua, Minh-Khoi Tran, and Sai-Kit Yeung. Point-wise convolutional neural network. In *Computer Vision and Pattern Recognition (CVPR)*, 2018.
- [15] Qiangui Huang, Weiyue Wang, and Ulrich Neumann. Recurrent slice networks for 3d segmentation on point clouds. In *Computer Vision and Pattern Recognition (CVPR)*, 2018.
- [16] Kibok Lee, Zhuoyuan Chen, Xinchun Yan, Raquel Urtasun, and Ersin Yumer. Shapeadv: Generating shape-aware adversarial 3d point clouds. *arXiv preprint arXiv:2005.11626*, 2020.
- [17] Yangyan Li, Rui Bu, Mingchao Sun, and Baoquan Chen. Pointcnn: Convolution on x-transformed points. *Advances in Neural Information Processing Systems (NIPS)*, 2018.
- [18] Daniel Liu, Ronald Yu, and Hao Su. Extending adversarial attacks and defenses to deep 3d point cloud classifiers. In *IEEE International Conference on Image Processing (ICIP)*, 2019.
- [19] Daniel Liu, Ronald Yu, and Hao Su. Adversarial point perturbations on 3d objects. In *European Conference on Computer Vision (ECCV) Workshop on Adversarial Robustness in the Real World*, 2020.
- [20] Xinhai Liu, Zhizhong Han, Yu-Shen Liu, and Matthias Zwicker. Point2sequence: Learning the shape representation of 3d point clouds with an attention-based sequence to sequence network. In *AAAI Conference on Artificial Intelligence (AAAI)*, 2019.
- [21] Apostolos Modas, Seyed-Mohsen Moosavi-Dezfooli, and Pascal Frossard. Sparsefool: A few pixels make a big difference. In *Computer Vision and Pattern Recognition (CVPR)*, 2019.
- [22] Nina Narodytska and Shiva Prasad Kasiviswanathan. Simple black-box adversarial perturbations for deep networks. *arXiv:1612.06299*, 2016.
- [23] B. K. Natarajan. Sparse approximate solutions to linear systems. *SIAM Journal on Computing*, 24(2):227–234, 1995.
- [24] Nicolas Papernot, Patrick McDaniel, Somesh Jha, Matt Fredrikson, Berkay Celik, and Ananthram Swami. The limitations of deep learning in adversarial settings. In *IEEE European Symposium on Security and Privacy*, 2016.
- [25] Adrien Poulenc, Marie-Julie Rakotosaona, Yann Ponty, and Maks Ovsjanikov. Effective rotation-invariant point cnn with spherical harmonics kernels. *International Conference on 3D Vision (3DV)*, 2019.
- [26] Charles Ruizhongtai Qi, Hao Su, Kaichun Mo, and Leonidas J Guibas. Pointnet: Deep learning on point sets for 3d classification and segmentation. In *Computer Vision and Pattern Recognition (CVPR)*, 2017.
- [27] Charles Ruizhongtai Qi, Li Yi, Hao Su, and Leonidas J Guibas. Pointnet++: Deep hierarchical feature learning on point sets in a metric space. In *Advances in Neural Information Processing Systems (NIPS)*, 2017.
- [28] Yongming Rao, Jiwen Lu, and Jie Zhou. Spherical fractal convolutional neural networks for point cloud recognition. In *Computer Vision and Pattern Recognition (CVPR)*, 2019.
- [29] Lukas Schott, Jonas Rauber, Matthias Bethge, and Wieland Brendel. Towards the first adversarially robust neural network model on MNIST. In *International Conference on Learning Representations (ICLR)*, 2019.
- [30] Yiru Shen, Chen Feng, Yaoqing Yang, and Dong Tian. Mining point cloud local structures by kernel correlation and

- graph pooling. In *Computer Vision and Pattern Recognition (CVPR)*, 2018.
- [31] Jiawei Su, Danilo Vasconcellos Vargas, and Kouichi Sakurai. One pixel attack for fooling deep neural networks. *IEEE Transactions on Evolutionary Computation*, 23(5):828–841, 2019.
- [32] Tzungyu Tsai, Kaichen Yang, Tsung-Yi Ho, and Yier Jin. Robust adversarial objects against deep learning models. In *AAAI Conference on Artificial Intelligence (AAAI)*, 2020.
- [33] Mikaela Angelina Uy, Quang-Hieu Pham, Binh-Son Hua, Duc Thanh Nguyen, and Sai-Kit Yeung. Revisiting point cloud classification: A new benchmark dataset and classification model on real-world data. In *International Conference on Computer Vision (ICCV)*, 2019.
- [34] Yue Wang, Yongbin Sun, Ziwei Liu, Sanjay E. Sarma, Michael M. Bronstein, and Justin M. Solomon. Dynamic graph cnn for learning on point clouds. *ACM Transactions on Graphics*, 38(5):1–12, 2019.
- [35] Yuxin Wen, Jiehong Lin, Ke Chen, and Kui Jia. Geometry-aware generation of adversarial and cooperative point clouds. In *arXiv:1902.10899*, 2019.
- [36] Matthew Wicker and Marta Kwiatkowska. Robustness of 3d deep learning in an adversarial setting. In *Computer Vision and Pattern Recognition (CVPR)*, 2019.
- [37] Ziyi Wu, Yueqi Duan, He Wang, Qingnan Fan, and Leonidas J Guibas. If-defense: 3d adversarial point cloud defense via implicit function based restoration. *arXiv preprint arXiv:2010.05272*, 2020.
- [38] Zhirong Wu, Shuran Song, Aditya Khosla, Fisher Yu, Linguang Zhang, Xiaoou Tang, and Jianxiong Xiao. 3d shapenets: A deep representation for volumetric shapes. In *Computer Vision and Pattern Recognition (CVPR)*, 2015.
- [39] Chong Xiang, Charles R. Qi, and Bo Li. Generating 3d adversarial point clouds. In *Computer Vision and Pattern Recognition (CVPR)*, 2019.
- [40] Yifan Xu, Tianqi Fan, Mingye Xu, Long Zeng, and Yu Qiao. Spidercnn: Deep learning on point sets with parameterized convolutional filters. In *European Conference on Computer Vision (ECCV)*, 2018.
- [41] Xu Yan, Chaoda Zheng, Zhen Li, Sheng Wang, and Shuguang Cui. Pointasnl: Robust point clouds processing using nonlocal neural networks with adaptive sampling. In *Computer Vision and Pattern Recognition (CVPR)*, 2020.
- [42] Jiancheng Yang, Qiang Zhang, Rongyao Fang, Bingbing Ni, Jinxian Liu, and Qi Tian. Adversarial attack and defense on point sets. In *arXiv:1902.10899*, 2019.
- [43] Yang You, Yujing Lou, Qi Liu, Yu-Wing Tai, Lizhuang Ma, Cewu Lu, and Weiming Wang. Pointwise rotation-invariant network with adaptive sampling and 3d spherical voxel convolution. In *AAAI Conference on Artificial Intelligence (AAAI)*, 2020.
- [44] Xiaoyong Yuan, Pan He, Qile Zhu, and Xiaolin Li. Adversarial examples: Attacks and defenses for deep learning. *IEEE Transactions on Neural Networks and Learning Systems*, 30(9):2805–2824, 2019.
- [45] Zhiyuan Zhang, Binh-Son Hua, David W. Rosen, and Sai-Kit Yeung. Rotation invariant convolutions for 3d point clouds deep learning. In *International Conference on 3D Vision (3DV)*, 2019.
- [46] Zhiyuan Zhang, Binh-Son Hua, and Sai-Kit Yeung. Shell-net: Efficient point cloud convolutional neural networks using concentric shells statistics. In *International Conference on Computer Vision (ICCV)*, 2019.
- [47] Yue Zhao, Yuwei Wu, Caihua Chen, and Andrew Lim. On isometry robustness of deep 3d point cloud models under adversarial attacks. In *Computer Vision and Pattern Recognition (CVPR)*, 2020.
- [48] Tianhang Zheng, Changyou Chen, Junsong Yuan, Bo Li, and Kui Ren. Pointcloud saliency maps. In *International Conference on Computer Vision (ICCV)*, 2019.
- [49] Hang Zhou, Dongdong Chen, Jing Liao, Kejiang Chen, Xiaoyi Dong, Kunlin Liu, Weiming Zhang, Gang Hua, and Nenghai Yu. Lg-gan: Label guided adversarial network for flexible targeted attack of point cloud based deep networks. In *Computer Vision and Pattern Recognition (CVPR)*, 2020.
- [50] Hang Zhou, Kejiang Chen, Weiming Zhang, Han Fang, Wenbo Zhou, and Nenghai Yu. Dup-net: Denoiser and up-sampler network for 3d adversarial point clouds defense. In *International Conference on Computer Vision (ICCV)*, 2019.

Supplementary Materials

Abstract

In this supplementary material, we present detailed derivations of the iterative gradient descent method used in our paper in Section A. We also report additional quantitative and qualitative results along with in-depth analyses and discussions on different aspects of our work. In particular, we verify the contributions of main components in our formulation, distance metrics, and initialisation of point selection in Section B. We report detailed performance of our adversarial attack algorithm on real-world data in Section C. We show how our adversarial point clouds can be defended in Section D. Finally, we present an experiment to verify the transferability of our adversarial examples across different point cloud networks in Section E.

A. Detailed Derivations

Recall that our adversarial examples are generated by minimising the objective function $f(P, \hat{\mathbf{a}}, E)$ defined in Eq. (8) in the paper. To solve this problem, we applied the iterative gradient descent methods in [11], which incrementally updates $\hat{\mathbf{a}}_i$ and \mathbf{e}_i as follows:

$$\begin{aligned}\hat{\mathbf{a}}_i^{(n+1)} &= \hat{\mathbf{a}}_i^{(n)} - \gamma \frac{\partial f}{\partial \hat{\mathbf{a}}_i} \\ \mathbf{e}_i^{(n+1)} &= \mathbf{e}_i^{(n)} - \gamma \frac{\partial f}{\partial \mathbf{e}_i}\end{aligned}$$

where $(\hat{\mathbf{a}}_i^{(n)}, \mathbf{e}_i^{(n)})$ is the solution at the n -th step and γ is set to 0.01 in our implementation.

We derive the partial derivatives $\frac{\partial f}{\partial \hat{\mathbf{a}}_i}$ and $\frac{\partial f}{\partial \mathbf{e}_i}$ as follows:

$$\begin{aligned}\frac{\partial f}{\partial \hat{\mathbf{a}}_i} &= \lambda_1 + \lambda_2 \frac{\partial D(P, P')}{\partial \hat{\mathbf{a}}_i} + \frac{\partial h(P')}{\partial \hat{\mathbf{a}}_i} \\ \frac{\partial f}{\partial \mathbf{e}_i} &= \lambda_2 \frac{\partial D(P, P')}{\partial \mathbf{e}_i} + \frac{\partial h(P')}{\partial \mathbf{e}_i}\end{aligned}$$

It can be seen that the calculations of $\frac{\partial f}{\partial \hat{\mathbf{a}}_i}$ and $\frac{\partial f}{\partial \mathbf{e}_i}$ require $\frac{\partial D(P, P')}{\partial \hat{\mathbf{a}}_i}$, $\frac{\partial D(P, P')}{\partial \mathbf{e}_i}$, $\frac{\partial h(P')}{\partial \hat{\mathbf{a}}_i}$, and $\frac{\partial h(P')}{\partial \mathbf{e}_i}$.

First, we present the calculations of $\frac{\partial D(P, P')}{\partial \hat{\mathbf{a}}_i}$ and $\frac{\partial D(P, P')}{\partial \mathbf{e}_i}$. As shown in our paper, we propose two ways to realise $D(P, P')$: using Chamfer distance and Hausdorff distance. For convenience in calculations, we rewrite $D(P, P')$ as follows,

$$D(P, P') = \max \left\{ D(P \rightarrow P'), D(P' \rightarrow P) \right\}$$

where, depending on the distance metric used, $D(P \rightarrow P')$ and $D(P' \rightarrow P)$ can be defined as,

$$D_{\text{Chamfer}}(P \rightarrow P') = \frac{1}{|P|} \sum_{\mathbf{p}_i \in P} \min_{\mathbf{p}'_j \in P'} \|\mathbf{p}_i - \mathbf{p}'_j\|_2$$

$$D_{\text{Chamfer}}(P' \rightarrow P) = \frac{1}{|P'|} \sum_{\mathbf{p}'_j \in P'} \min_{\mathbf{p}_i \in P} \|\mathbf{p}'_j - \mathbf{p}_i\|_2$$

$$D_{\text{Hausdorff}}(P \rightarrow P') = \max_{\mathbf{p}_i \in P} \min_{\mathbf{p}'_j \in P'} \|\mathbf{p}_i - \mathbf{p}'_j\|_2$$

$$D_{\text{Hausdorff}}(P' \rightarrow P) = \max_{\mathbf{p}'_j \in P'} \min_{\mathbf{p}_i \in P} \|\mathbf{p}'_j - \mathbf{p}_i\|_2$$

Next, we obtain,

$$\frac{\partial D(P, P')}{\partial \hat{\mathbf{a}}_i} = \begin{cases} \frac{\partial D(P \rightarrow P')}{\partial \hat{\mathbf{a}}_i} & \text{if } D(P \rightarrow P') \geq D(P' \rightarrow P) \\ \frac{\partial D(P' \rightarrow P)}{\partial \hat{\mathbf{a}}_i} & \text{otherwise} \end{cases}$$

$$\frac{\partial D(P, P')}{\partial \mathbf{e}_i} = \begin{cases} \frac{\partial D(P \rightarrow P')}{\partial \mathbf{e}_i} & \text{if } D(P \rightarrow P') \geq D(P' \rightarrow P) \\ \frac{\partial D(P' \rightarrow P)}{\partial \mathbf{e}_i} & \text{otherwise} \end{cases}$$

For Chamfer distance, we have,

$$\frac{\partial D_{\text{Chamfer}}(P \rightarrow P')}{\partial \hat{\mathbf{a}}_i} = \frac{1}{|P|} \sum_{\mathbf{p}_k \in P} \frac{\partial}{\partial \hat{\mathbf{a}}_i} (\min_{\mathbf{p}'_j \in P'} \|\mathbf{p}_k - \mathbf{p}'_j\|_2)$$

$$\frac{\partial D_{\text{Chamfer}}(P \rightarrow P')}{\partial \mathbf{e}_i} = \frac{1}{|P|} \sum_{\mathbf{p}_k \in P} \frac{\partial}{\partial \mathbf{e}_i} (\min_{\mathbf{p}'_j \in P'} \|\mathbf{p}_k - \mathbf{p}'_j\|_2)$$

where

$$\begin{aligned}& \frac{\partial}{\partial \hat{\mathbf{a}}_i} (\min_{\mathbf{p}'_j \in P'} \|\mathbf{p}_k - \mathbf{p}'_j\|_2) \\ &= \begin{cases} \frac{\mathbf{e}_i^\top (\mathbf{p}'_i - \mathbf{p}_k)}{\|\mathbf{p}'_i - \mathbf{p}_k\|_2} & \text{if } \mathbf{p}'_i = \underset{\mathbf{p}'_j \in P'}{\operatorname{argmin}} \|\mathbf{p}_k - \mathbf{p}'_j\|_2 \\ 0 & \text{otherwise} \end{cases} \\ & \frac{\partial}{\partial \mathbf{e}_i} (\min_{\mathbf{p}'_j \in P'} \|\mathbf{p}_k - \mathbf{p}'_j\|_2) \\ &= \begin{cases} \frac{\hat{\mathbf{a}}_i (\mathbf{p}'_i - \mathbf{p}_k)}{\|\mathbf{p}'_i - \mathbf{p}_k\|_2} & \text{if } \mathbf{p}'_i = \underset{\mathbf{p}'_j \in P'}{\operatorname{argmin}} \|\mathbf{p}_k - \mathbf{p}'_j\|_2 \\ 0 & \text{otherwise} \end{cases}\end{aligned}$$

For Hausdorff distance, we have,

$$\begin{aligned}& \frac{\partial D_{\text{Hausdorff}}(P \rightarrow P')}{\partial \hat{\mathbf{a}}_i} \\ &= \begin{cases} \frac{\mathbf{e}_i^\top (\mathbf{p}'_i - \mathbf{p}_k)}{\|\mathbf{p}'_i - \mathbf{p}_k\|_2} & \text{if } \|\mathbf{p}_k - \mathbf{p}'_i\|_2 = \max_{\mathbf{p}_l \in P} \min_{\mathbf{p}'_j \in P'} \|\mathbf{p}_l - \mathbf{p}'_j\|_2 \\ 0 & \text{otherwise} \end{cases} \\ & \frac{\partial D_{\text{Hausdorff}}(P \rightarrow P')}{\partial \mathbf{e}_i} \\ &= \begin{cases} \frac{\hat{\mathbf{a}}_i (\mathbf{p}'_i - \mathbf{p}_k)}{\|\mathbf{p}'_i - \mathbf{p}_k\|_2} & \text{if } \|\mathbf{p}_k - \mathbf{p}'_i\|_2 = \max_{\mathbf{p}_l \in P} \min_{\mathbf{p}'_j \in P'} \|\mathbf{p}_l - \mathbf{p}'_j\|_2 \\ 0 & \text{otherwise} \end{cases}\end{aligned}$$

We note that $\frac{\partial D_{Chamfer}(P' \rightarrow P)}{\partial \hat{a}_i}$, $\frac{\partial D_{Chamfer}(P' \rightarrow P)}{\partial \mathbf{e}_i}$, $\frac{\partial D_{Hausdorff}(P' \rightarrow P)}{\partial \hat{a}_i}$, $\frac{\partial D_{Hausdorff}(P' \rightarrow P)}{\partial \mathbf{e}_i}$ can be calculated similarly.

Finally, we compute $\frac{\partial h(P')}{\partial \hat{a}_i}$ and $\frac{\partial h(P')}{\partial \mathbf{e}_i}$ as follows,

$$\begin{aligned}\frac{\partial h(P')}{\partial \hat{a}_i} &= \frac{\partial h(P')}{\partial \mathbf{p}'_i} \frac{\partial \mathbf{p}'_i}{\partial \hat{a}_i} = \mathbf{e}_i^\top \frac{\partial h(P')}{\partial \mathbf{p}'_i} \\ \frac{\partial h(P')}{\partial \mathbf{e}_i} &= \frac{\partial h(P')}{\partial \mathbf{p}'_i} \frac{\partial \mathbf{p}'_i}{\partial \mathbf{e}_i} = \hat{a}_i \frac{\partial h(P')}{\partial \mathbf{p}'_i}\end{aligned}$$

where $\frac{\partial h(P')}{\partial \mathbf{p}'_i}$ is achievable from a target point cloud network. For instance, PointNet applies multi-layer perceptrons on points individually, which support the calculations of $\frac{\partial h(P')}{\partial \mathbf{p}'_i}$, for every point $\mathbf{p}'_i \in P'$.

B. Ablation Study

B.1. Sparsity vs Perceptibility

We performed an in-depth analysis of our formulation by studying its constituting components. In particular, we investigated the role of the sparsity term, i.e., $\|\hat{\mathbf{a}}\|_1$, and the perceptibility term, i.e., $D(P, P')$, in Eq. (8) in our paper. In this experiment, we set λ_1 and λ_2 to 0, respectively, and measured the corresponding performances of attacks.

We report the performance of our method in terms of the success rate (of attack), the Chamfer distances and Hausdorff distances of generated samples to original samples, and the average numbers of points used in point perturbation and point addition in Table 5.

As shown in our experimental results, when the sparsity is not considered, i.e., $\lambda_1 = 0$, the adversarial generation method achieves higher attack rates but requires considerably high numbers of points. In contrast, when the perceptibility is not used, i.e., $\lambda_2 = 0$, relatively lower success rates are incurred (compared with $\lambda_1 = 0$), much lesser numbers of points are used but adversarial examples much deform from original point clouds (as shown in the Hausdorff distances). This phenomenon can be explained by the following imaginary experiment: take a few (even one) points on an input point cloud and move those points much away from the original point cloud. It is obvious to see that this perturbation will significantly change the shape of the point cloud and thus will affect any point cloud classification methods. However, such extreme samples can also be detected easily by using outlier or noise removal methods, e.g., [18].

In the current implementation of our adversarial attack, we set $\lambda_1 = 0.15$ and $\lambda_2 = 50$. We notice on the difference in the values of λ_1 and λ_2 , which is caused by the difference in the range of values of their associated terms. In particular, $\|\hat{\mathbf{a}}\|_1$ captures the number of manipulated points, which varies in $[0, 1024]$ while $D(P, P') \in [0, 1]$ since point clouds are normalised into $[0, 1]$ before being pro-

cessed. We empirically observed minor changes in the attack performance of our method for $\lambda_1 \in [0.1, 0.2]$ and $\lambda_2 \in [30, 50]$ while the current settings gave the best balance for many contradictory criteria including minimal attack, high success rate, and reasonable perceptibility. We show several results illustrating the effects of the sparsity and perceptibility of adversarial examples in Figure 5.

B.2. Chamfer Distance vs Hausdorff Distance

We experimented our method with Chamfer and Hausdorff distance, i.e., replacing $D(P, P')$ by $D_{Chamfer}(P, P')$ and $D_{Hausdorff}(P, P')$, respectively in Eq. (4) and Eq. (5) in our paper. Table 6 shows attack results of these two distance metrics in point perturbation and point addition attack. Note that the two columns labelled as ‘‘Chamfer Distance’’ and ‘‘Hausdorff Distance’’ in Table 6 report the Chamfer and Hausdorff distances from generated adversarial examples to original point clouds. As shown in the results, there is little difference in the numbers of manipulated points between Chamfer and Hausdorff distance in both point perturbation and point addition attack. On one hand, Chamfer distance shows higher success rate. On the other hand, Hausdorff distance better preserves the perceptibility of point clouds during point manipulation.

We visually show adversarial examples generated by using Chamfer distance and Hausdorff distance in Figure 6. We qualitatively observed that attacks using Chamfer distance often place a few points far away from original point clouds, making high success rate but low perceptibility. In addition, we empirically found that adversarial examples, whose Hausdorff distance to their original point clouds is over 0.01, often include obvious outliers and thus are detectable easily. However, a comprehensive user-study on human perception of adversarial examples would better reflect the perceptibility of these distance metrics, and thus is worthwhile for future research.

B.3. Initialisation of Point Selection

Similarly to point perturbation attacks presented in our paper, we experimented point addition attacks with different initialisation schemes for point selection including: critical points-based initialisation (i.e., using critical points from [26] to initialise added points), all points-based initialisation (i.e., considering all points in a point cloud as added points), and random points-based initialisation.

We report the performance of these initialisation schemes in Table 7. Our results show that, like point perturbation, compared with critical points-based initialisation and all points-based initialisation, random points-based initialisation balance the success rate and number of points while ensuring the perceptibility of adversarial examples.

	Success Rate	Chamfer Distance	Hausdorff Distance	# Points
Perturbation $\lambda_1=0$	99.67	2.06×10^{-3}	4.58×10^{-2}	536
Perturbation $\lambda_2=0$	98.53	9.03×10^{-4}	3.61×10^{-1}	6
Addition $\lambda_1=0$	98.62	8.46×10^{-4}	4.75×10^{-2}	986
Addition $\lambda_2=0$	99.03	1.19×10^{-3}	4.22×10^{-1}	6

(a) Modelnet40

	Success Rate	Chamfer Distance	Hausdorff Distance	# Points
Perturbation $\lambda_1=0$	99.29	1.72×10^{-3}	3.55×10^{-2}	542
Perturbation $\lambda_2=0$	97.16	6.59×10^{-4}	3.22×10^{-1}	7
Addition $\lambda_1=0$	98.81	6.73×10^{-4}	3.44×10^{-2}	983
Addition $\lambda_2=0$	98.81	7.32×10^{-4}	3.45×10^{-1}	6

(b) ScanObjectNN

Table 5: Comparison of point sparsity and object perceptibility in generating adversarial examples in point perturbation and point addition on both synthetic and real-world data.

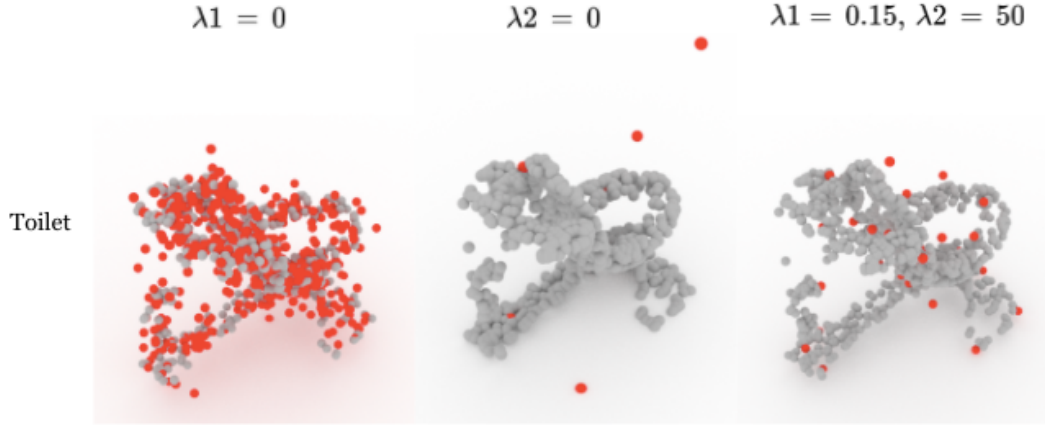


Figure 5: Adversarial examples generated using different settings.

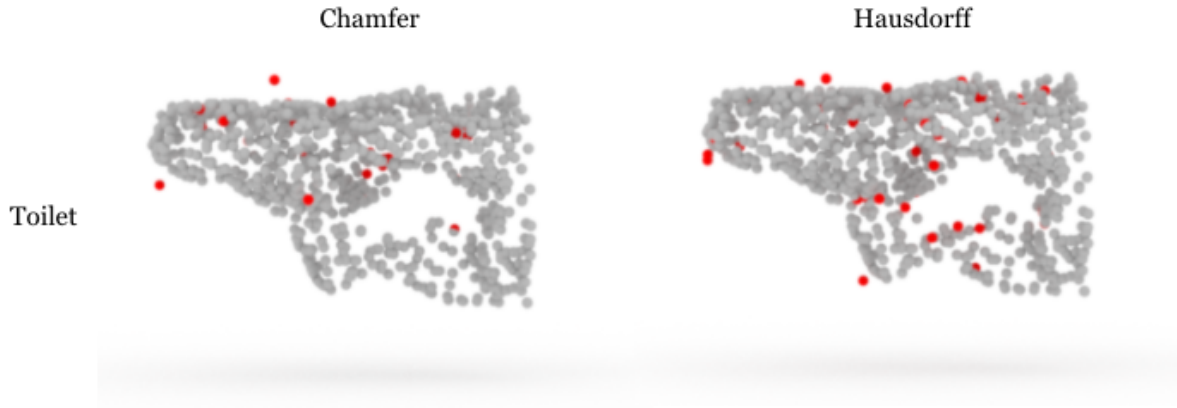


Figure 6: Chamfer Distance vs Hausdorff Distance.

	Success Rate	Chamfer Distance	Hausdorff Distance	# Points
Chamfer	98.35	2.94×10^{-4}	9.03×10^{-2}	42
Hausdorff	89.38	1.55×10^{-4}	1.88×10^{-2}	36
(a) Perturbation attack on Modelnet40				
	Success Rate	Chamfer Distance	Hausdorff Distance	# Points
Chamfer	97.71	3.36×10^{-4}	1.09×10^{-1}	34
Hausdorff	89.01	1.53×10^{-4}	1.98×10^{-2}	38
(b) Addition attack on Modelnet40				
	Success Rate	Chamfer Distance	Hausdorff Distance	# Points
Chamfer	96.69	1.89×10^{-4}	6.51×10^{-2}	42
Hausdorff	91.72	1.12×10^{-4}	1.15×10^{-2}	34
(c) Perturbation attack on ScanObjectNN				
	Success Rate	Chamfer Distance	Hausdorff Distance	# Points
Chamfer	97.87	1.99×10^{-4}	7.27×10^{-2}	37
Hausdorff	90.44	1.08×10^{-4}	1.10×10^{-2}	38
(d) Addition attack on ScanObjectNN				

Table 6: Attack performance of distance method on Modelnet40 and ScanObjectNN.

	Success Rate	Chamfer Distance	Hausdorff Distance	# Points
Critical points	90.07	1.06×10^{-4}	1.03×10^{-2}	30
Using all points	92.67	1.22×10^{-4}	1.16×10^{-2}	65
Ours (random points)	90.44	1.08×10^{-4}	1.10×10^{-2}	38

Table 7: Point addition attack performance with different point initialisation strategies on ScanObjectNN.

C. Attack Performance on Real-World Data

We also evaluated our method on the entire real-world dataset, ScanObjectNN. Recall that ScanObjectNN has five variants corresponding to five challenges. Specifically, “OBJ_BG” includes objects with background, “PB_T25” includes objects translated by 25%, post-fixes “R” and “S” denote rotated and scaled objects, respectively. Readers are referred to [33] for more details of ScanObjectNN dataset.

We report the attack performance of our method to PointNet on the entire ScanObjectNN dataset in Table 8. As shown in results, our method maintains a success rate of more than 90% by using only 4% of total points. Our method also performs consistently across all the variants of ScanObjectNN. Furthermore, we observe that, amongst all the variants, OBJ_BG appears to be the most challenging one (i.e., low success rate and high level of deformation, as shown in Hausdorff distances). This observation is also consistent with conclusion from [33], indicating that OBJ_BG is the most difficult variant for object recognition.

We show several results of our method on the OBJ_BG

variant and entire ScannObjectNN dataset in Figure 7 and Figure 8 respectively. In general, compared with the results from existing works, our adversarial examples look more natural, perturbed and added points visually look like common noise and thus are hard to be noticed (without being highlighted). This suggests the necessity to validate attack techniques in extreme situations, e.g., with minimal attacks.

D. Defense

We experimented adversarial defense to our adversarial point clouds. In this experiment, we implemented two defense techniques in [18]: outlier removal and salient point removal. The outlier removal technique first estimates statistical outliers from a point set and then removes points that have large standard deviations. The salient point removal operates by first estimating point saliency and then removing points in the order from high to low saliency.

We show defense results in Table 9. In general, it is moderately easy to defend adversarial point clouds using the above methods, with a success rate up to 94% for adversar-

Variant	Success Rate	Chamfer Distance	Hausdorff Distance	# Points
OBJ_BG	91.72	1.12×10^{-4}	1.15×10^{-2}	34
PB_T25	94.04	9.74×10^{-4}	1.12×10^{-2}	33
PB_T25_R	91.09	9.53×10^{-5}	1.02×10^{-2}	31
PB_T50_R	90.58	8.59×10^{-5}	9.61×10^{-3}	30
PB_T50_RS	91.92	7.68×10^{-5}	8.77×10^{-3}	27

(a) Point Perturbation

Variant	Success Rate	Chamfer Distance	Hausdorff Distance	# Points
OBJ_BG	90.44	1.08×10^{-4}	1.10×10^{-2}	38
PB_T25	93.62	1.13×10^{-4}	1.26×10^{-2}	36
PB_T25_R	92.13	9.06×10^{-5}	9.76×10^{-3}	34
PB_T50_R	92.29	8.18×10^{-5}	9.24×10^{-3}	32
PB_T50_RS	92.43	7.51×10^{-5}	8.73×10^{-3}	30

(b) Point Addition

Table 8: Attack performance to PointNet on entire ScanObjectNN.

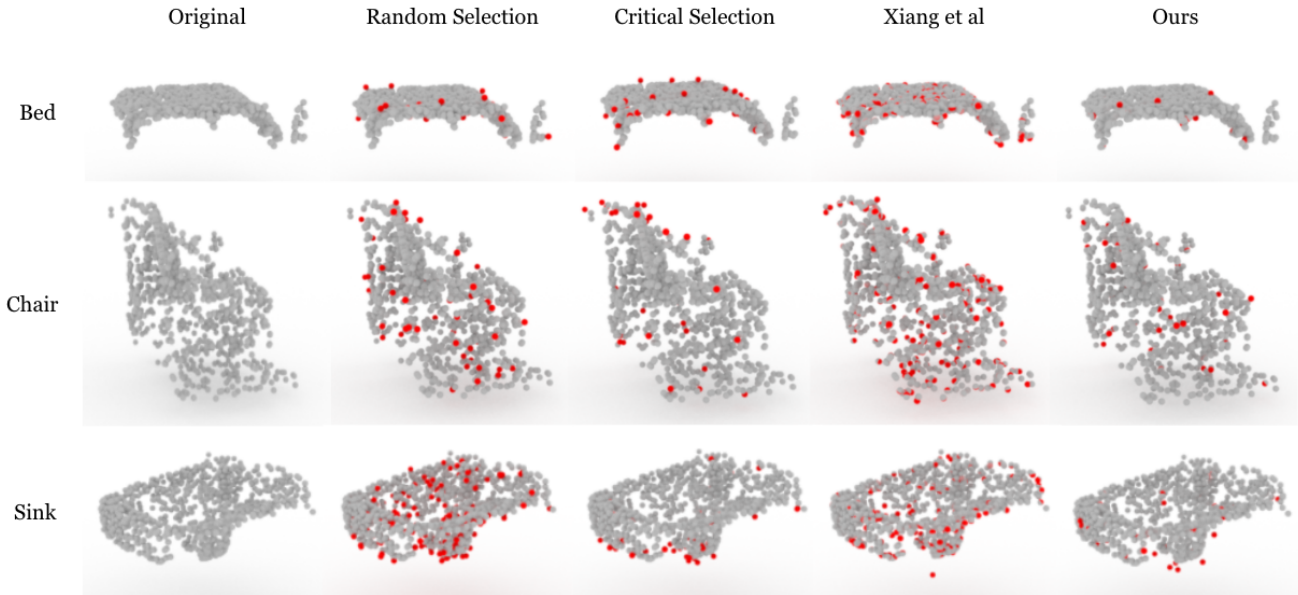


Figure 7: Adversarial examples of point addition attack on OBJ_BG. Added points are highlighted in red.

ial examples in ModelNet40. Despite that, we found such defenses on real world data in ScanObjectNN are less effective, e.g., the success rate decreases on harder variants of ScanObjectNN. However, the salient point removal method works pretty well on cases with severe object deformations, e.g., the variants PB_50_R and PB_50_RS. This is because points added by the point addition attack could be close to salient points and thus noticed by the salient point removal method. It would also be useful to study how to make adversarial examples with minimal attacks on salient points.

E. Transferability

In this experiment, we investigated the transferability of adversarial examples across different point cloud networks. Specifically, we fed adversarial point clouds generated with PointNet [26] as the target network to PointNet++ [27] for attacks. In the opposite way, we transferred adversarial examples generated using PointNet++ to PointNet.

We report the success rates of cross-network adversarial example transfers for both point perturbation and point addition on ModelNet40 and OBJ_BG of ScanObjectNN in

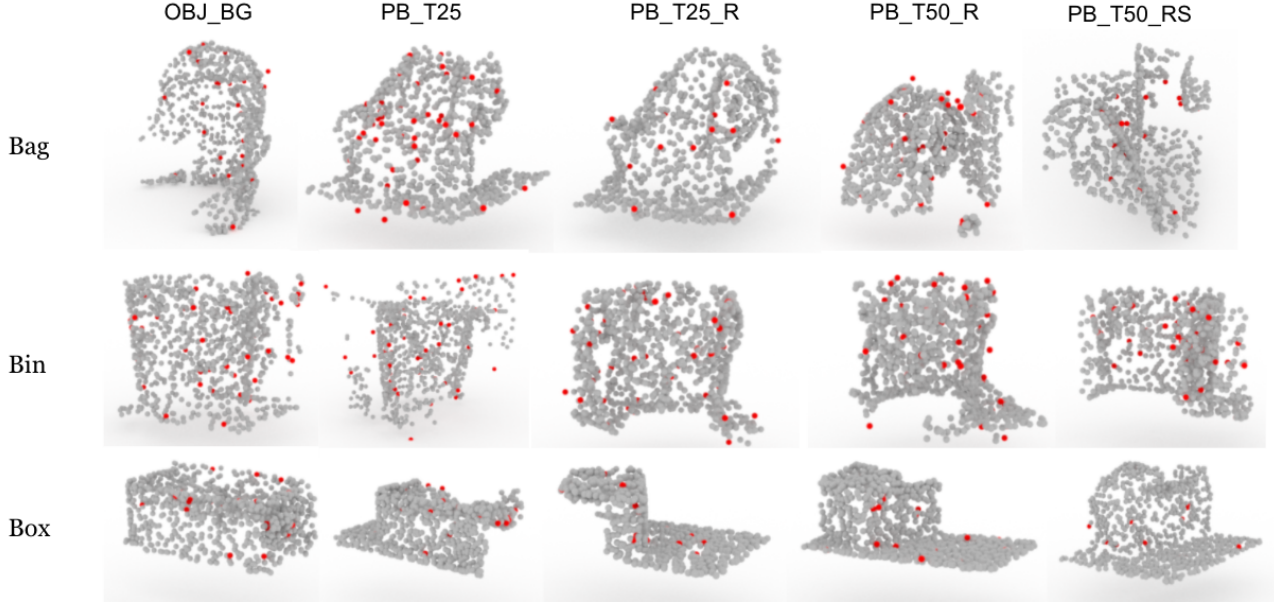


Figure 8: Adversarial examples of point perturbation attack on ScanObjectNN. Perturbed points are highlighted in red.

	Success Rate	Outlier removal [18]	Salient point removal [18]
Modelnet40	89.38	95.55	95.4
OBJ_BG	91.72	94.32	96.64
PB_T25	94.04	91.83	93.72
PB_T25_R	91.09	91	93.81
PB_T50_R	90.58	90.35	93.49
PB_T50_RS	91.92	89.13	93.35
(a) Perturbation			
	Success Rate	Outlier removal [18]	Salient point removal [18]
Modelnet40	89.01	94.21	96.31
OBJ_BG	90.44	93.12	96.56
PB_T25	93.62	90.34	94.24
PB_T25_R	92.13	89.31	94.34
PB_T50_R	92.29	88.68	93.5
PB_T50_RS	92.43	87.79	93.5
(b) Addition			

Table 9: Defense performance.

Table 10. We found that both point perturbation and point addition attack are challenging to cross-network transfers. For instance, the attack success rates in both ways: PointNet to PointNet++ and PointNet++ to PointNet, are about 20s% on both Modelnet40 and OBJ_BG. This observation is also consistent to that by Xiang et al. [39].

	Point Perturbation	Point Addition
ModelNet40	7.68	6.49
OBJ_BG	25.75	25.11
(a) PointNet to PointNet++		
	Point Perturbation	Point Addition
ModelNet40	25.66	22.34
OBJ_BG	19.55	20.94
(b) PointNet++ to PointNet		

16 Table 10: Cross-network adversarial example transfer. While the success rates are low, the results suggest that real-world data is more vulnerable to black box attacks.

An interesting observation from experimental results is that real-world adversarial examples in ScanObjectNN are easier to transfer than synthetic examples in ModelNet40, which makes real-world data more vulnerable to black box attacks. This also suggests the need to further enhance the robustness of 3D point cloud networks.